# Review on Multirate Feedforward Control with Mode Decomposition for Intersample Performance in Multi-Modal Motion Systems

Masahiro Mae*a) Student Member, Wataru Ohnishi* Member
Hiroshi Fujimoto* Senior Member

Multirate feedforward control enables perfect tracking control for the desired state trajectory at every sample as the same number of the model order. The aim of this paper is the comparison of perfect tracking control approaches for intersample performance in multi-modal motion systems. The multirate feedforward control has a trade-off between the number of states for perfect tracking control and the reference sampling frequency. To balance the trade-off, the states for the perfect tracking control can be selected by the mode decomposition. Intersample performance of each approach in a multi-modal motion system is compared in both frequency domain and time domain.

**Keywords:** multirate feedforward control, perfect tracking control, zero-order-hold, mode decomposition, intersample performance

## 1. Introduction

Feedforward control based on exact model inversion enables perfect tracking control [1] for the model of the controlled system. The quality of the feedforward controller directly results in tracking performance in high-precision mechatronic systems such as wafer scanners [2], wire bonders [3], and ball-screw-driven stages [4]. In industrial applications, the system is controlled in discrete time but the tracking performance should be improved in continuous time.

The exact model inversion has a challenge when the model has nonminimum-phase zeros such as intrinsic and discretization zeros [5]. The single-rate stable inversion approach [6] generates the noncausal bounded feedforward input for the model with nonminimum-phase zeros and provides perfect output tracking for every sample. However, it cannot compensate for the zeros around $-1$ that cause the oscillating input and deteriorate intersample performance.

To improve intersample performance, the multirate feedforward control [7,8] is presented. The multirate feedforward control provides perfect $n$ states tracking for every $n$ samples and prevents intersample oscillation. There is a trade-off in the multirate feedforward control between the number of states for perfect tracking control and the reference sampling frequency. To balance the trade-off, the multirate feedforward control approaches based on modal form with additive decomposition [9, 10] and multiplicative decomposition [11] are presented. Both approaches select the states for perfect tracking control and balance the trade-off to improve intersample performance.

Although several approaches are available to design the perfect tracking controller, the choice of the feedforward controller can be arbitrarily and there is no comparison in terms of intersample performance for perfect tracking controllers. The aim of this paper is the analysis of pre-existing perfect tracking controllers in both frequency domain and time domain and provides the guideline to design the feedforward controller to improve intersample performance. The main contributions of this paper are as follows.

(1) Perfect tracking control approaches are described focusing on improving intersample performance in multi-modal motion systems.
(2) Intersample performance of each approach is validated in both frequency domain and time domain.

a) Correspondence to: mmae@ieee.org
* The University of Tokyo
5-1-5, Kashiwanoha, Kashiwa, Chiba, Japan

## 2. Problem formulation

### 2.1 Intersample performance in sampled-data control

The considered tracking control configuration is shown in Figure 1, with reference $r \in \mathbb{R}$, input $u \in \mathbb{R}$, output $y \in \mathbb{R}$, and error $e \in \mathbb{R}$. The $n^{\text{th}}$ order continuous-time linear time-invariant system $G_c \overset{s}{=} (\boldsymbol{A}_c, \boldsymbol{b}_c, \boldsymbol{c}_c, 0)$ is given by

$$\dot{\boldsymbol{x}}(t) = \boldsymbol{A}_c \boldsymbol{x}(t) + \boldsymbol{b}_c u(t), \quad \cdots (1)$$

$$y(t) = \boldsymbol{c}_c \boldsymbol{x}(t). \quad \cdots (2)$$

The discrete-time system $\boldsymbol{H}_d \overset{z}{=} (\boldsymbol{A}_d, \boldsymbol{B}_d, \boldsymbol{C}_d, \boldsymbol{D}_d)$ of the continuous-time system $\boldsymbol{H}_c \overset{s}{=} (\boldsymbol{A}_c, \boldsymbol{B}_c, \boldsymbol{C}_c, \boldsymbol{D}_c)$ discretized by sampler $\mathcal{S}$ and zero-order-hold $\mathcal{H}$ in sampling time $\delta$ is generally defined as

$$\left[\begin{array}{c|c} \boldsymbol{A}_d & \boldsymbol{B}_d \\ \hline \boldsymbol{C}_d & \boldsymbol{D}_d \end{array}\right] = \left[\begin{array}{c|c} e^{\boldsymbol{A}_c \delta} & \boldsymbol{A}_c^{-1}(e^{\boldsymbol{A}_c \delta} - \boldsymbol{I})\boldsymbol{B}_c \\ \hline \boldsymbol{C}_c & \boldsymbol{D}_c \end{array}\right], \quad \cdots (3)$$

$$\boldsymbol{x}[k] = \boldsymbol{x}(k\delta). \quad \cdots (4)$$

The discrete-time system $G_d \overset{z}{=} (\boldsymbol{A}_d, \boldsymbol{b}_d, \boldsymbol{c}_d, 0) = \mathcal{S} G_c \mathcal{H}$ is given by

$$\dot{\boldsymbol{x}}[k+1] = \boldsymbol{A}_d \boldsymbol{x}[k] + \boldsymbol{b}_d u[k], \quad \cdots (5)$$

$$y[k] = \boldsymbol{c}_d \boldsymbol{x}[k]. \quad \cdots (6)$$

The control objective considered in this paper is to minimize the continuous-time error $e(t)$ that includes both on-sample and intersample performance for the continuous-time reference $r(t)$ that is assumed to be known in advance.

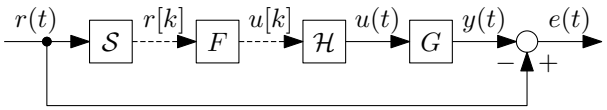


Fig. 1. Block diagram of tracking control. The continuous-time system $G$ is controlled by the discrete-time controller $F$ with sampler $\mathcal{S}$ and zero-order-hold $\mathcal{H}$. The objective is to minimize the continuous-time error $e(t)$.

**2.2 Single-rate feedforward control based on discrete-time model inversion** The one-sample forward shifted system $\tilde{G}_d$ of $G_d$ from $u[k]$ to $y[k+1]$ is given by

$$\boldsymbol{x}[k+1] = \boldsymbol{A}_d\boldsymbol{x}[k] + \boldsymbol{b}_d u[k], \cdots\cdots\cdots\cdots\cdots\cdots (7)$$

$$y[k+1] = \boldsymbol{c}_d\boldsymbol{A}_d\boldsymbol{x}[k] + \boldsymbol{c}_d\boldsymbol{b}_d u[k]. \cdots\cdots\cdots\cdots\cdots\cdots (8)$$

For the system $\boldsymbol{H} = (\boldsymbol{A}, \boldsymbol{B}, \boldsymbol{C}, \boldsymbol{D})$ with nonsingular $\boldsymbol{D}$, the inverse system $\boldsymbol{H}^{-1}$ is generally defined as

$$\boldsymbol{H}^{-1} = \left[\begin{array}{c|c} \boldsymbol{A} - \boldsymbol{B}\boldsymbol{D}^{-1}\boldsymbol{C} & \boldsymbol{B}\boldsymbol{D}^{-1} \\ \hline -\boldsymbol{D}^{-1}\boldsymbol{C} & \boldsymbol{D}^{-1} \end{array}\right]. \cdots\cdots\cdots\cdots (9)$$

By inverting $\tilde{G}_d$, the input $u$ generated by the single-rate feedforward controller is given by

$$u[k] = \tilde{G}_d^{-1} r[k+1], \cdots\cdots\cdots\cdots\cdots\cdots\cdots\cdots (10)$$

where the single-rate feedforward controller $\tilde{G}_d^{-1}$ is given by

$$\tilde{G}_d^{-1} = \left[\begin{array}{c|c} \boldsymbol{A}_d - \boldsymbol{b}_d(\boldsymbol{c}_d\boldsymbol{b}_d)^{-1}\boldsymbol{c}_d\boldsymbol{A}_d & \boldsymbol{b}_d(\boldsymbol{c}_d\boldsymbol{b}_d)^{-1} \\ \hline -(\boldsymbol{c}_d\boldsymbol{b}_d)^{-1}\boldsymbol{c}_d\boldsymbol{A}_d & (\boldsymbol{c}_d\boldsymbol{b}_d)^{-1} \end{array}\right]. \cdot (11)$$

When $\tilde{G}_d^{-1}$ has unstable poles, it can be decomposed as

$$\begin{bmatrix} \boldsymbol{x}_s[k+1] \\ \boldsymbol{x}_u[k+1] \end{bmatrix} = \begin{bmatrix} \boldsymbol{A}_s & \boldsymbol{O} \\ \boldsymbol{O} & \boldsymbol{A}_u \end{bmatrix} \begin{bmatrix} \boldsymbol{x}_s[k] \\ \boldsymbol{x}_u[k] \end{bmatrix} + \begin{bmatrix} \boldsymbol{b}_s \\ \boldsymbol{b}_u \end{bmatrix} r[k+1], \cdot (12)$$

$$u[k] = \begin{bmatrix} \boldsymbol{c}_s & \boldsymbol{c}_u \end{bmatrix} \begin{bmatrix} \boldsymbol{x}_s[k] \\ \boldsymbol{x}_u[k] \end{bmatrix} + dr[k+1], \cdots\cdots (13)$$

where $|\lambda(\boldsymbol{A}_s)| \le 1$ and $|\lambda(\boldsymbol{A}_u)| > 1$. The bounded feedforward input $u$ is given by

$$u[k] = \boldsymbol{c}_s\boldsymbol{x}_s[k] + \boldsymbol{c}_u\boldsymbol{x}_u[k] + dr[k+1] \cdots\cdots\cdots\cdots (14)$$

where $\boldsymbol{x}_s$ follows from solving

$$\boldsymbol{x}_s[k+1] = \boldsymbol{A}_s\boldsymbol{x}_s[k] + \boldsymbol{b}_s r[k+1],\ \boldsymbol{x}_s[-\infty] = \boldsymbol{0} \cdots (15)$$

forward in time and $\boldsymbol{x}_u$ follows from solving

$$\boldsymbol{x}_u[k+1] = \boldsymbol{A}_u\boldsymbol{x}_u[k] + \boldsymbol{b}_u r[k+1],\ \boldsymbol{x}_u[\infty] = \boldsymbol{0} \cdots (16)$$

backward in time [6]. The generated feedforward input $u$ provides perfect output tracking for every sample.

Note that although the feedforward input generated by the single-rate stable inversion approach is bounded, the oscillating poles around $\lambda = -1$ cannot be compensated. The oscillating feedforward input can deteriorate intersample performance.

**2.3 Multirate feedforward control for full-state tracking** To compensate for oscillating poles of the feedforward controller due to discretization, multirate feedforward control [7] based on perfect state tracking is presented.

The $n$ samples lifted system $\underline{\boldsymbol{H}}_d$ of $\boldsymbol{H}_d \overset{z}{=} (\boldsymbol{A}_d, \boldsymbol{B}_d, \boldsymbol{C}_d, \boldsymbol{D}_d)$ is generally defined as

$$\underline{\boldsymbol{H}}_d \overset{z^n}{=} \mathcal{L}_n\boldsymbol{H}_d\mathcal{L}_n^{-1} = \left[\begin{array}{c|c} \underline{\boldsymbol{A}}_d & \underline{\boldsymbol{B}}_d \\ \hline \underline{\boldsymbol{C}}_d & \underline{\boldsymbol{D}}_d \end{array}\right]$$

$$= \left[\begin{array}{c|ccccc} \boldsymbol{A}_d^n & \boldsymbol{A}_d^{n-1}\boldsymbol{B}_d & \boldsymbol{A}_d^{n-2}\boldsymbol{B}_d & \cdots & \boldsymbol{A}_d\boldsymbol{B}_d & \boldsymbol{B}_d \\ \hline \boldsymbol{C}_d & \boldsymbol{D}_d & \boldsymbol{O} & \cdots & \cdots & \boldsymbol{O} \\ \boldsymbol{C}_d\boldsymbol{A}_d & \boldsymbol{C}_d\boldsymbol{B}_d & \boldsymbol{D}_d & \ddots & & \vdots \\ \vdots & \vdots & \ddots & \ddots & \ddots & \vdots \\ \boldsymbol{C}_d\boldsymbol{A}_d^{n-2} & \boldsymbol{C}_d\boldsymbol{A}_d^{n-3}\boldsymbol{B}_d & \boldsymbol{C}_d\boldsymbol{A}_d^{n-4}\boldsymbol{B}_d & \ddots & \boldsymbol{D}_d & \boldsymbol{O} \\ \boldsymbol{C}_d\boldsymbol{A}_d^{n-1} & \boldsymbol{C}_d\boldsymbol{A}_d^{n-2}\boldsymbol{B}_d & \boldsymbol{C}_d\boldsymbol{A}_d^{n-3}\boldsymbol{B}_d & \cdots & \boldsymbol{C}_d\boldsymbol{B}_d & \boldsymbol{D}_d \end{array}\right] \cdots (17)$$

$$\underline{u}[i_n] = \mathcal{L}_n u[k] = \begin{bmatrix} u[ni_n] & \cdots & u[ni_n + (n-1)] \end{bmatrix}^{\mathsf{T}} \in \mathbb{R}^n, \cdot (18)$$

$$\underline{y}[i_n] = \mathcal{L}_n y[k] = \begin{bmatrix} y[ni_n] & \cdots & y[ni_n + (n-1)] \end{bmatrix}^{\mathsf{T}} \in \mathbb{R}^n, \cdot (19)$$

where $\mathcal{L}_n$ is $n$ samples lifting operator [12].

The $n$ samples lifted system of $G_d$ is given by

$$\underline{G}_d \overset{z^n}{=} \mathcal{L}_n G_d \mathcal{L}_n^{-1} = \left[\begin{array}{c|c} \underline{\boldsymbol{A}}_d & \underline{\boldsymbol{B}}_d \\ \hline \underline{\boldsymbol{C}}_d & \underline{\boldsymbol{D}}_d \end{array}\right]. \cdots\cdots\cdots\cdots (20)$$

The desired state trajectory of $\underline{G}_d$ is given by the multirate sampler for every $n$ samples $\mathcal{S}_n$ that is defined as

$$\hat{\boldsymbol{x}}[i_n] = \mathcal{S}_n\hat{\boldsymbol{x}}(t) = \hat{\boldsymbol{x}}(i_n n\delta), \cdots\cdots\cdots\cdots\cdots\cdots (21)$$

where $\hat{\boldsymbol{x}}(t)$ is the desired state trajectory in continuous time. By inverting the state equation of $\underline{G}_d$, the input $u$ generated by the multirate feedforward controller is given by

$$\begin{aligned} u[k] &= \mathcal{L}_n^{-1}\left(\underline{\boldsymbol{B}}_d^{-1}\hat{\boldsymbol{x}}[i_n+1] - \underline{\boldsymbol{B}}_d^{-1}\underline{\boldsymbol{A}}_d\hat{\boldsymbol{x}}[i_n]\right) \\ &= \mathcal{L}_n^{-1}\underline{\boldsymbol{B}}_d^{-1}(\boldsymbol{I} - z^{-n}\underline{\boldsymbol{A}}_d)\hat{\boldsymbol{x}}[i_n+1], \cdots\cdots\cdots\cdots (22) \end{aligned}$$

where $z$ is shift operator in sampling time $\delta$. The generated feedforward input $u$ provides perfect state tracking for every $n$ samples and improves intersample performance.

Note that the desired state trajectory $\hat{\boldsymbol{x}}$ is given by the reference and its derivatives in continuous time for the system without zeros in controllable canonical form. When the system has zeros, the desired state trajectory generation method is described in the next section. Although the multirate feedforward controller provides perfect state tracking for every $n$ samples, the sampling time of the desired state trajectory is $n\delta$, and the higher the model order $n$ is, the lower the reference sampling frequency $1/n\delta$ is.

**2.4 Problem description** From these discussions, the optimal perfect tracking controller should be designed by considering the following requirements.

(1) Oscillating poles of the feedforward controller due to discretization is compensated by state tracking.

(2) States for perfect tracking control are selected to make reference sampling frequency enough high.

The state tracking can be provided by multirate feedforward control and the states can be selected based on the mode decomposition. In this paper, two kinds of multirate feedforward controllers with mode selection in additive decomposition [9, 10] and multiplicative decomposition [11] are described and intersample performance is compared with preexisting perfect tracking control approaches.

## 3. Desired state trajectory generation

The single-input single-output continuous-time linear time-invariant $n^{\text{th}}$ order system is given by

$$G_c(s) = \frac{B(s)}{A(s)} = \frac{b_m s^m + \cdots + b_1 s + b_0}{s^n + a_{n-1}s^{n-1} + \cdots + a_1 s + a_0}, \cdot (23)$$

where $n > m$ and $b_0 \neq 0$. $G_c$ in controllable canonical form $G_{c,ccf} \overset{s}{=} (\boldsymbol{A}_{c,ccf}, \boldsymbol{b}_{c,ccf}, \boldsymbol{c}_{c,ccf}, 0)$ is given by

$$\dot{\boldsymbol{x}}_{ccf}(t) = \boldsymbol{A}_{c,ccf}\boldsymbol{x}_{ccf}(t) + \boldsymbol{b}_{c,ccf}u(t), \cdots\cdots\cdots\cdots (24)$$
$$y(t) = \boldsymbol{c}_{c,ccf}\boldsymbol{x}_{ccf}(t), \cdots\cdots\cdots\cdots\cdots\cdots (25)$$

where

$$\left[\begin{array}{c|c} \boldsymbol{A}_{c,ccf} & \boldsymbol{b}_{c,ccf} \\ \hline \boldsymbol{c}_{c,ccf} & 0 \end{array}\right] = \left[\begin{array}{cccc|c} 0 & 1 & & 0 & 0 \\ & \ddots & \ddots & & \vdots \\ 0 & & 0 & 1 & 0 \\ -a_0 & \cdots & \cdots & -a_{n-1} & 1 \\ \hline b_0 & \cdots & b_m & 0 & 0 \end{array}\right]. (26)$$

The filter for the state trajectory generation is given by

$$\beta(t) = \mathcal{L}^{-1}\left[B(s)^{-1}\right], \cdots\cdots\cdots\cdots\cdots\cdots (27)$$

where $\mathcal{L}[\cdot]$ is the unilateral Laplace transform. The desired state trajectory in the controllable canonical form is given by

$$\hat{\boldsymbol{x}}_{ccf}(t) = \int_0^t \beta(t-\tau)\bar{r}_n(\tau)\mathrm{d}\tau, \cdots\cdots\cdots\cdots (28)$$

where

$$\hat{\boldsymbol{x}}_{ccf}(t) = \left[\hat{x}_{ccf}(t) \quad \cdots \quad \hat{x}_{ccf,n-1}(t)\right]^\mathsf{T}, \cdots\cdots\cdots (29)$$
$$\bar{r}_n(t) = \left[1 \quad \cdots \quad \frac{\mathrm{d}^{n-1}}{\mathrm{d}t^{n-1}}\right]^\mathsf{T} r(t). \cdots\cdots\cdots\cdots (30)$$

When $B(s)^{-1}$ has unstable poles, it can be decomposed as

$$B(s)^{-1} = B_s^{-1}(s) + B_u^{-1}(s), \cdots\cdots\cdots\cdots\cdots (31)$$

where all poles $p_s \in \mathbb{C}$ of $B_s^{-1}(s)$ are $\mathrm{Re}(p_s) \leq 0$ and all poles $p_u \in \mathbb{C}$ of $B_u^{-1}(s)$ are $\mathrm{Re}(p_u) > 0$. The filters of stable and unstable parts for the state trajectory generation are given by

$$\beta_s(t) = \mathcal{L}^{-1}\left[B_s^{-1}(s)\right], \cdots\cdots\cdots\cdots\cdots (32)$$
$$\beta_u(t) = \mathcal{L}^{-1}\left[B_u^{-1}(-s)\right]. \cdots\cdots\cdots\cdots\cdots (33)$$

The stable and unstable parts of the desired state trajectory are given by

$$\hat{\boldsymbol{x}}_s(t) = \int_{-\infty}^t \beta_s(t-\tau)\bar{r}_n(\tau)\mathrm{d}\tau, \cdots\cdots\cdots\cdots (34)$$
$$\hat{\boldsymbol{x}}_u(t) = \int_t^\infty \beta_u(t-\tau)\bar{r}_n(\tau)\mathrm{d}\tau, \cdots\cdots\cdots\cdots (35)$$

and the bounded desired state trajectory in controllable canonical form $\hat{\boldsymbol{x}}_{ccf}$ is given by

$$\hat{\boldsymbol{x}}_{ccf}(t) = \hat{\boldsymbol{x}}_s(t) + \hat{\boldsymbol{x}}_u(t). \cdots\cdots\cdots\cdots\cdots (36)$$

## 4. Multirate feedforward control with mode decomposition

**4.1 Definition of multi-modal motion system** The continuous-time multi-modal motion system is defined as

$$G_c(s) = \sum_{k_m=1}^{n_m} \frac{\kappa_{k_m}}{s^2 + 2\zeta_{k_m}\omega_{k_m}s + \omega_{k_m}^2} = \sum_{k_m=1}^{n_m} G_{c,mod,k_m}(s), (37)$$

where $\omega$, $\zeta$, $\kappa$, and $n_m$ are the resonance angle frequency, the damping coefficient, the mode gain, and the number of modes, respectively [13]. $G_c$ in modal form $G_{c,mod} \overset{s}{=} (\boldsymbol{A}_{c,mod}, \boldsymbol{b}_{c,mod}, \boldsymbol{c}_{c,mod}, 0)$ is given by

$$\dot{\boldsymbol{x}}_{mod}(t) = \boldsymbol{A}_{c,mod}\boldsymbol{x}_{mod}(t) + \boldsymbol{b}_{c,mod}u(t), \cdots\cdots\cdots (38)$$
$$y(t) = \boldsymbol{c}_{c,mod}\boldsymbol{x}_{mod}(t), \cdots\cdots\cdots\cdots\cdots (39)$$

where

$$\left[\begin{array}{c|c} \boldsymbol{A}_{c,mod} & \boldsymbol{b}_{c,mod} \\ \hline \boldsymbol{c}_{c,mod} & 0 \end{array}\right] = \left[\begin{array}{ccc|c} \boldsymbol{A}_{c,mod,1} & & \boldsymbol{O} & \boldsymbol{b}_{c,mod,1} \\ & \ddots & & \vdots \\ \boldsymbol{O} & & \boldsymbol{A}_{c,mod,n_m} & \boldsymbol{b}_{c,mod,n_m} \\ \hline \boldsymbol{c}_{c,mod,1} & \cdots & \boldsymbol{c}_{c,mod,n_m} & 0 \end{array}\right], (40)$$

$$\boldsymbol{x}_{mod}(t) = \left[\boldsymbol{x}_{mod,1}(t) \quad \cdots \quad \boldsymbol{x}_{mod,n_m}(t)\right]^\mathsf{T}, \cdots\cdots\cdots (41)$$

and the subsystem $G_{c,mod,k_m} \overset{s}{=} (\boldsymbol{A}_{c,mod,k_m}, \boldsymbol{b}_{c,mod,k_m}, \boldsymbol{c}_{c,mod,k_m}, 0)$ is given by

$$\left[\begin{array}{c|c} \boldsymbol{A}_{c,mod,k_m} & \boldsymbol{b}_{c,mod,k_m} \\ \hline \boldsymbol{c}_{c,mod,k_m} & 0 \end{array}\right] = \left[\begin{array}{cc|c} 0 & 1 & 0 \\ -\omega_{k_m}^2 & -2\zeta_{k_m}\omega_{k_m} & 1 \\ \hline \kappa_{k_m} & 0 & 0 \end{array}\right]. (42)$$

$$\boldsymbol{x}_{mod,k_m}(t) = \left[x_{mod,k_m,0}(t) \quad x_{mod,k_m,1}(t)\right]^\mathsf{T}. \cdots\cdots\cdots (43)$$

The state transformation of the system $\boldsymbol{H} = (\boldsymbol{A}, \boldsymbol{B}, \boldsymbol{C}, \boldsymbol{D})$ with the state transformation matrix $\boldsymbol{T}$ is generally defined as

$$\mathcal{T}(\boldsymbol{H}, \boldsymbol{T}) = \left[\begin{array}{c|c} \boldsymbol{T}\boldsymbol{A}\boldsymbol{T}^{-1} & \boldsymbol{T}\boldsymbol{B} \\ \hline \boldsymbol{C}\boldsymbol{T}^{-1} & \boldsymbol{D} \end{array}\right]. \cdots\cdots\cdots\cdots (44)$$

The state transformation matrix $\boldsymbol{T}_{mod}$ from controllable canonical form to modal form is given by

$$\boldsymbol{T}_{mod} = \left[\boldsymbol{b}_{c,mod} \quad \cdots \quad \boldsymbol{A}_{c,mod}^{n-1}\boldsymbol{b}_{c,mod}\right]\left[\begin{array}{cccc} a_1 & \cdots & a_{n-1} & 1 \\ \vdots & \iddots & \iddots & \\ a_{n-1} & \iddots & & \\ 1 & & & \boldsymbol{O} \end{array}\right], \cdots (45)$$

where

$$G_{c,mod} = \mathcal{T}(G_{c,ccf}, \boldsymbol{T}_{mod}), \cdots\cdots\cdots\cdots\cdots (46)$$
$$\boldsymbol{x}_{mod}(t) = \boldsymbol{T}_{mod}\boldsymbol{x}_{ccf}(t). \cdots\cdots\cdots\cdots\cdots (47)$$

**4.2 Multirate feedforward control with additive decomposition** The overview of multirate feedforward control with additive decomposition is shown in Figure 2. The indices $\mu$ of the selected modes are defined as

$$\mu = \{k_m | k_m \in 1, \ldots, n_m\}, \cdots\cdots\cdots\cdots\cdots (48)$$

and the order $\nu$ of the selected modes is defined as

$$\nu = 2 \times \mathrm{number}\{\mu\}. \cdots\cdots\cdots\cdots\cdots (49)$$

The permutation matrix for the selected modes is defined as

$$\boldsymbol{T}_\mu = \left[\begin{array}{c} \boldsymbol{E}_\mu \\ \boldsymbol{E}_\times \end{array}\right], \cdots\cdots\cdots\cdots\cdots (50)$$

where $\boldsymbol{E}_\mu$ and $\boldsymbol{E}_\times$ consist of standard basis vectors of selected and unselected modes, and the standard basis vectors of the mode $k_m$ is defined as

$$\boldsymbol{E}_{k_m} = \left[\boldsymbol{O}_{2\times 2(k_m-1)} \quad \boldsymbol{I}_2 \quad \boldsymbol{O}_{2\times 2(n_m-k_m)}\right]. \cdots\cdots\cdots (51)$$

The model reduction matrix extracting upper $\nu$ states is defined as

$$\boldsymbol{T}_\nu = \left[\boldsymbol{I}_\nu \quad \boldsymbol{O}_{\nu\times(n-\nu)}\right]. \cdots\cdots\cdots\cdots\cdots (52)$$

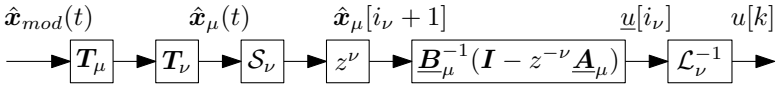


Fig. 2. Block diagram of multirate feedforward control with additive decomposition.

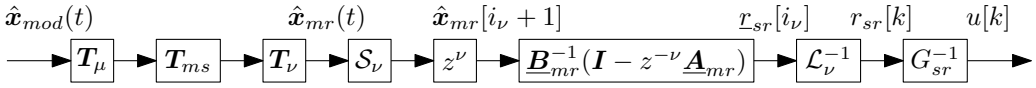


Fig. 3. Block diagram of multirate feedforward control with multiplicative decomposition.

The system of the selected modes $G_{c,\mu}$ is given by

$$\dot{\boldsymbol{x}}_\mu(t) = \boldsymbol{A}_{c,\mu}\boldsymbol{x}_\mu(t) + \boldsymbol{b}_{c,\mu}u(t), \quad \cdots\cdots (53)$$
$$y(t) = \boldsymbol{c}_{c,\mu}\boldsymbol{x}_\mu(t), \quad \cdots\cdots (54)$$

where

$$\boldsymbol{x}_\mu(t) = \boldsymbol{T}_\nu\boldsymbol{T}_\mu\boldsymbol{x}_{mod}(t), \quad \cdots\cdots (55)$$
$$\boldsymbol{A}_{c,\mu} = \boldsymbol{T}_\nu\boldsymbol{T}_\mu\boldsymbol{A}_{c,mod}\boldsymbol{T}_\mu^{-1}\boldsymbol{T}_\nu^{\mathsf{T}}, \quad \cdots\cdots (56)$$
$$\boldsymbol{b}_{c,\mu} = \boldsymbol{T}_\nu\boldsymbol{T}_\mu\boldsymbol{b}_{c,mod}, \quad \cdots\cdots (57)$$
$$\boldsymbol{c}_{c,\mu} = \boldsymbol{c}_{c,mod}\boldsymbol{T}_\mu^{-1}\boldsymbol{T}_\nu^{\mathsf{T}}. \quad \cdots\cdots (58)$$

The discrete-time system of $G_{c,\mu}$ is given by

$$G_{d,\mu} \overset{z}{=} \mathcal{S}G_{c,\mu}\mathcal{H} = \left[\begin{array}{c|c} \boldsymbol{A}_{d,\mu} & \boldsymbol{b}_{d,\mu} \\ \hline \boldsymbol{c}_{d,\mu} & 0 \end{array}\right], \quad \cdots\cdots (59)$$

and the $\nu$ samples lifted system of $G_{d,\mu}$ is given by

$$\underline{G}_{d,\mu} \overset{z^\nu}{=} \mathcal{L}_\nu G_{d,\mu}\mathcal{L}_\nu^{-1} = \left[\begin{array}{c|c} \underline{\boldsymbol{A}}_{d,\mu} & \underline{\boldsymbol{B}}_{d,\mu} \\ \hline \underline{\boldsymbol{C}}_{d,\mu} & \underline{\boldsymbol{D}}_{d,\mu} \end{array}\right]. \quad \cdots\cdots (60)$$

By inverting the state equation of $\underline{G}_{d,\mu}$, the input $u$ generated by the multirate feedforward controller with additive decomposition is given by

$$\begin{aligned} u[k] &= \mathcal{L}_\nu^{-1}\left(\underline{\boldsymbol{B}}_{d,\mu}^{-1}\hat{\boldsymbol{x}}_\mu[i_\nu+1] - \underline{\boldsymbol{B}}_{d,\mu}^{-1}\underline{\boldsymbol{A}}_{d,\mu}\hat{\boldsymbol{x}}_\mu[i_\nu]\right) \\ &= \mathcal{L}_\nu^{-1}\underline{\boldsymbol{B}}_{d,\mu}^{-1}(\boldsymbol{I}-z^{-\nu}\underline{\boldsymbol{A}}_{d,\mu})\hat{\boldsymbol{x}}_\mu[i_\nu+1], \quad \cdots\cdots (61) \end{aligned}$$

where $\hat{\boldsymbol{x}}_\mu[i_\nu] = \mathcal{S}_\nu\boldsymbol{T}_\nu\boldsymbol{T}_\mu\hat{\boldsymbol{x}}_{mod}(t)$. The generated feedforward input $u$ provides perfect state tracking for every $\nu$ samples for the states corresponding to the selected modes $\mu$.

Note that although perfect state tracking for selected states does not guarantee perfect output tracking, it can provide better intersample performance because the desired state trajectory is generated by the model with full states and the reference sampling frequency for selected $\nu$ ($\leq n$) states becomes higher from $1/n\delta$ to $1/\nu\delta$.

**4.3 Multirate feedforward control with multiplicative decomposition** The overview of multirate feedforward control with multiplicative decomposition is shown in Figure 3. The one-sample forward shifted system $\tilde{G}_{d,mod} \overset{z}{=} (\tilde{\boldsymbol{A}}_{d,mod}, \tilde{\boldsymbol{b}}_{d,mod}, \tilde{\boldsymbol{c}}_{d,mod}, \tilde{d}_{d,mod})$ of the discrete-time system in modal form $G_{d,mod} \overset{z}{=} (\boldsymbol{A}_{d,mod}, \boldsymbol{b}_{d,mod}, \boldsymbol{c}_{d,mod}, 0) = \mathcal{S}G_{c,mod}\mathcal{H}$ from $u[k]$ to $y[k+1]$ is given by

$$\left[\begin{array}{c|c} \tilde{\boldsymbol{A}}_{d,mod} & \tilde{\boldsymbol{b}}_{d,mod} \\ \hline \tilde{\boldsymbol{c}}_{d,mod} & \tilde{d}_{d,mod} \end{array}\right] = \left[\begin{array}{c|c} \boldsymbol{A}_{d,mod} & \boldsymbol{b}_{d,mod} \\ \hline \boldsymbol{c}_{d,mod}\boldsymbol{A}_{d,mod} & \boldsymbol{c}_{d,mod}\boldsymbol{b}_{d,mod} \end{array}\right]. \quad (62)$$

When $\nu$ states corresponding to the modes $\mu$ are selected,

$$\boldsymbol{\Pi} = \boldsymbol{S}\begin{bmatrix} \boldsymbol{I}_\nu & \boldsymbol{O}_{\nu\times(n-\nu)} \\ \boldsymbol{O}_{(n-\nu)\times\nu} & \boldsymbol{O}_{(n-\nu)} \end{bmatrix}\boldsymbol{S}^{-1} \quad \cdots\cdots (63)$$

is defined with full rank $\boldsymbol{S} = \begin{bmatrix} \boldsymbol{V} & \boldsymbol{V}_\times \end{bmatrix}$, where $\boldsymbol{V} \in \mathbb{R}^{n\times\nu}$ and $\boldsymbol{V}_\times \in \mathbb{R}^{n\times(n-\nu)}$ are a column space of an invariant subspace of $\boldsymbol{A} = \tilde{\boldsymbol{A}}_{d,mod}$ and $\boldsymbol{A}_\times = \tilde{\boldsymbol{A}}_{d,mod} - \tilde{\boldsymbol{b}}_{d,mod}\tilde{d}_{d,mod}^{-1}\tilde{\boldsymbol{c}}_{d,mod}$ that correspond to the poles of $G_{mr}$ and the zeros of $G_{sr}$. Then the state-space realizations are given by

$$G_{mrf} \overset{z}{=} \left[\begin{array}{c|c} \tilde{\boldsymbol{A}}_{d,mod} & \boldsymbol{\Pi}\tilde{\boldsymbol{b}}_{d,mod}\tilde{d}_{d,mod}^{-1} \\ \hline \tilde{\boldsymbol{c}}_{d,mod} & 1 \end{array}\right], \quad \cdots\cdots (64)$$

$$G_{srf} \overset{z}{=} \left[\begin{array}{c|c} \tilde{\boldsymbol{A}}_{d,mod} & \tilde{\boldsymbol{b}}_{d,mod} \\ \hline \tilde{\boldsymbol{c}}_{d,mod}(\boldsymbol{I}-\boldsymbol{\Pi}) & \tilde{d}_{d,mod} \end{array}\right]. \quad \cdots\cdots (65)$$

Let the permutation matrix $\boldsymbol{T}_\mu$ be such that

$$\mathcal{T}(G_{mrf}, \boldsymbol{T}_\mu) \overset{z}{=} \left[\begin{array}{cc|c} \boldsymbol{A}_{mr} & \boldsymbol{O} & \boldsymbol{b}_{mr} \\ \boldsymbol{O} & \boldsymbol{A}_{sr} & \boldsymbol{0} \\ \hline \boldsymbol{c}_{mr} & \boldsymbol{c}_{mrr} & 1 \end{array}\right], \quad \cdots\cdots (66)$$

$$\mathcal{T}(G_{srf}, \boldsymbol{T}_\mu) \overset{z}{=} \left[\begin{array}{cc|c} \boldsymbol{A}_{mr} & \boldsymbol{O} & \boldsymbol{b}_{srr} \\ \boldsymbol{O} & \boldsymbol{A}_{sr} & \boldsymbol{b}_{sr} \\ \hline \boldsymbol{0} & \boldsymbol{c}_{sr} & d_{sr} \end{array}\right]. \quad \cdots\cdots (67)$$

$G_{mr}$ with states $\boldsymbol{x}_{mr}$ and $G_{sr}$ with states $\boldsymbol{x}_{sr}$ are given by

$$G_{mr} \overset{z}{=} \left[\begin{array}{c|c} \boldsymbol{A}_{mr} & \boldsymbol{b}_{mr} \\ \hline \boldsymbol{c}_{mr} & 1 \end{array}\right], \quad \cdots\cdots (68)$$

$$G_{sr} \overset{z}{=} \left[\begin{array}{c|c} \boldsymbol{A}_{sr} & \boldsymbol{b}_{sr} \\ \hline \boldsymbol{c}_{sr} & d \end{array}\right]. \quad \cdots\cdots (69)$$

The product of the system $\boldsymbol{H}_1 = (\boldsymbol{A}_1, \boldsymbol{B}_1, \boldsymbol{C}_1, \boldsymbol{D}_1)$ and $\boldsymbol{H}_2 = (\boldsymbol{A}_2, \boldsymbol{B}_2, \boldsymbol{C}_2, \boldsymbol{D}_2)$ is generally defined as

$$\boldsymbol{H}_1\boldsymbol{H}_2 = \left[\begin{array}{cc|c} \boldsymbol{A}_1 & \boldsymbol{B}_1\boldsymbol{C}_2 & \boldsymbol{B}_1\boldsymbol{D}_2 \\ \boldsymbol{O} & \boldsymbol{A}_2 & \boldsymbol{B}_2 \\ \hline \boldsymbol{C}_1 & \boldsymbol{D}_1\boldsymbol{C}_2 & \boldsymbol{D}_1\boldsymbol{D}_2 \end{array}\right]. \quad \cdots\cdots (70)$$

The state transformation matrix $\boldsymbol{T}_{ms}$ is given by

$$\boldsymbol{T}_{ms} = \begin{bmatrix} \boldsymbol{I}_\nu & \boldsymbol{X} \\ \boldsymbol{O}_{\nu\times(n-\nu)} & \boldsymbol{I}_{(n-\nu)} \end{bmatrix}^{-1}, \quad \cdots\cdots (71)$$

where $\boldsymbol{X} \in \mathbb{R}^{\nu\times(n-\nu)}$ is the solution of the Sylvester equation

$$\boldsymbol{A}_{mr}\boldsymbol{X} - \boldsymbol{X}\boldsymbol{A}_{sr} = \boldsymbol{b}_{mr}\boldsymbol{c}_{sr}. \quad \cdots\cdots (72)$$

$\tilde{G}_{ms} \overset{z}{=} (\tilde{\boldsymbol{A}}_{ms}, \tilde{\boldsymbol{b}}_{ms}, \tilde{\boldsymbol{c}}_{ms}, d) = \mathcal{T}(\tilde{G}_{d,mod}, \boldsymbol{T}_{ms}\boldsymbol{T}_\mu) = G_{mr}G_{sr}$ is given by

$$\left[\begin{array}{c|c} \tilde{\boldsymbol{A}}_{ms} & \tilde{\boldsymbol{b}}_{ms} \\ \hline \tilde{\boldsymbol{c}}_{ms} & d \end{array}\right] = \left[\begin{array}{cc|c} \boldsymbol{A}_{mr} & \boldsymbol{b}_{mr}\boldsymbol{c}_{sr} & \boldsymbol{b}_{mr}d \\ \boldsymbol{O} & \boldsymbol{A}_{sr} & \boldsymbol{b}_{sr} \\ \hline \boldsymbol{c}_{mr} & \boldsymbol{c}_{sr} & d \end{array}\right]. \quad \cdots\cdots (73)$$

The $\nu$ samples lifted system of $G_{mr}$ is given by

$$\underline{G}_{mr} \overset{z^\nu}{=} \mathcal{L}_\nu G_{mr}\mathcal{L}_\nu^{-1} = \left[\begin{array}{c|c} \underline{\boldsymbol{A}}_{mr} & \underline{\boldsymbol{B}}_{mr} \\ \hline \underline{\boldsymbol{C}}_{mr} & 0 \end{array}\right]. \quad \cdots\cdots (74)$$

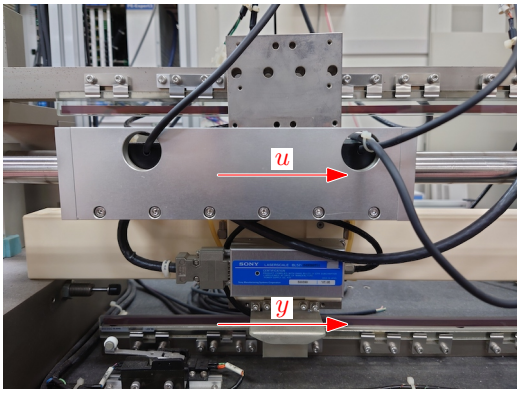


Fig. 4. High-precision positioning stage with input current $u$ [A] generating force with linear motor and output displacement $y$ [m] measured by linear encoder.

By inverting the state equation of $\underline{G}_{mr}$, the reference for the single-rate inversion $r_{sr}$ is given by

$$\begin{aligned} r_{sr}[k] &= \mathcal{L}_\nu^{-1}\left(\underline{\boldsymbol{B}}_{d,mr}^{-1}\hat{\boldsymbol{x}}_{mr}[i_\nu+1] - \underline{\boldsymbol{B}}_{d,mr}^{-1}\underline{\boldsymbol{A}}_{d,mr}\hat{\boldsymbol{x}}_{mr}[i_\nu]\right) \\ &= \mathcal{L}_\nu^{-1}\underline{\boldsymbol{B}}_{d,mr}^{-1}(\boldsymbol{I} - z^{-\nu}\underline{\boldsymbol{A}}_{d,mr})\hat{\boldsymbol{x}}_{mr}[i_\nu+1], \quad \cdots\cdots (75) \end{aligned}$$

where $\hat{\boldsymbol{x}}_\mu[i_\nu] = \mathcal{S}_\nu \boldsymbol{T}_\nu \boldsymbol{T}_{ms} \boldsymbol{T}_\mu \hat{\boldsymbol{x}}_{mod}(t)$. Then, the input $u$ generated by the multirate feedforward controller with multiplicative decomposition is given by

$$u[k] = G_{sr}^{-1} r_{sr}[k], \cdots\cdots (76)$$

where

$$G_{sr}^{-1} = \left[\begin{array}{c|c} \boldsymbol{A}_{sr} - \boldsymbol{b}_{sr} d_{sr}^{-1} \boldsymbol{c}_{sr} & \boldsymbol{b}_{sr} d_{sr}^{-1} \\ \hline -d_{sr}^{-1}\boldsymbol{c}_{sr} & d_{sr}^{-1} \end{array}\right]. \cdots\cdots (77)$$

Note that the one-sample backward shifted system of $\tilde{G}_{ms}$ is given by

$$\begin{aligned} G_{ms} &= \mathcal{T}(G_{d,mod}, \boldsymbol{T}_{ms}\boldsymbol{T}_\mu) = \left[\begin{array}{c|c} \boldsymbol{A}_{ms} & \boldsymbol{b}_{ms} \\ \hline \boldsymbol{c}_{ms} & 0 \end{array}\right] \\ &= \left[\begin{array}{c|c} \tilde{\boldsymbol{A}}_{ms} & \tilde{\boldsymbol{b}}_{ms} \\ \hline \tilde{\boldsymbol{c}}_{ms}\tilde{\boldsymbol{A}}_{ms}^{-1} & 0 \end{array}\right] = \left[\begin{array}{cc|c} \boldsymbol{A}_{mr} & \boldsymbol{b}_{mr}\boldsymbol{c}_{sr} & \boldsymbol{b}_{mr}d \\ \boldsymbol{O} & \boldsymbol{A}_{sr} & \boldsymbol{b}_{sr} \\ \hline \boldsymbol{c}_{mr}^* & d_{mr}^*\boldsymbol{c}_{sr}^* & d_{mr}^* d \end{array}\right] \\ &= \left[\begin{array}{c|c} \boldsymbol{A}_{mr} & \boldsymbol{b}_{mr} \\ \hline \boldsymbol{c}_{mr}^* & d_{mr}^* \end{array}\right]\left[\begin{array}{c|c} \boldsymbol{A}_{sr} & \boldsymbol{b}_{sr} \\ \hline \boldsymbol{c}_{sr}^* & d \end{array}\right], \cdots\cdots (78) \end{aligned}$$

where $d_{mr}^* d = 0$ and the output is given by

$$y[k] = \boldsymbol{c}_{mr}^* \boldsymbol{x}_{mr}[k] + d_{mr}^* \boldsymbol{c}_{sr}^* \boldsymbol{x}_{sr}[k]. \cdots\cdots (79)$$

It shows that the approach provides perfect output tracking for every $\nu$ samples with $d_{mr}^* = 0$ because the multirate inversion provides perfect state tracking of $\boldsymbol{x}_{mr}$ for every $\nu$ samples. If the system is decomposed as $d_{mr}^* \neq 0$, there is no perfect output tracking because perfect state tracking of $\boldsymbol{x}_{sr}$ is not guaranteed. Therefore, $\boldsymbol{V}$ and $\boldsymbol{V}_\times$ should be selected such that $d_{mr}^* = 0$.

## 5. Verification in multi-modal motion system

**5.1 Conditions** The verification is conducted in a multi-modal motion system in Figure 4 that is given by

$$G_c(s) = \frac{2.44}{s^2} + \frac{1.1}{s^2 + 2\times 0.024 \times (2\pi\times 30)s + (2\pi\times 30)^2}$$

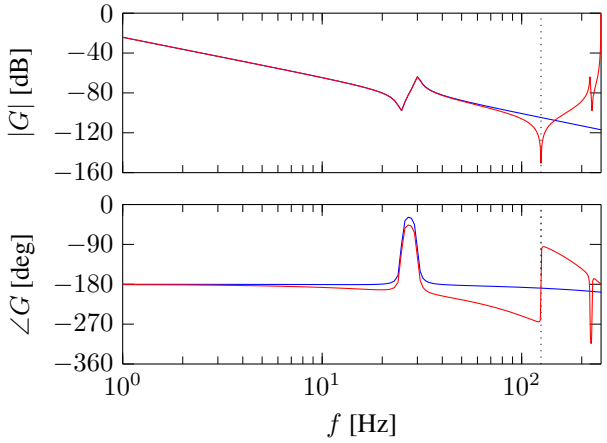


Fig. 5. Bode diagram of controlled system: continuous–time model $G_c$ (—), and discrete-time model $G_d$ (—). Nyquist frequency is shown in a vertical black dotted line (····).

$$\begin{aligned} &= G_{c,mod,1}(s) + G_{c,mod,2}(s) \cdots\cdots (80) \\ &= \frac{3.54}{s^2} \times \frac{s^2 + 2\times 0.02 \times (2\pi\times 25)s + (2\pi\times 25)^2}{s^2 + 2\times 0.024 \times (2\pi\times 30)s + (2\pi\times 30)^2} \\ &= \frac{N_1(s)}{D_1(s)} \times \frac{N_2(s)}{D_2(s)}. \cdots\cdots (81) \end{aligned}$$

The sampling time is $\delta = 4$ ms. The continuous-time model $G_c$ and the discrete-time model $G_d$ are shown in Figure 5. The compared 8 approaches are summarized in Table 1.

**5.2 Verification in frequency domain** Intersample performance is verified by the performance frequency gain $|E_r|$ that is the steady state continuous-time tracking error normalized by the step sine wave reference and is defined as

$$|E_r(\mathrm{j}\omega)| = \frac{\mathrm{RMS}(e_{\mathrm{j}\omega}(t))}{\mathrm{RMS}(r_{\mathrm{j}\omega}(t))}, \cdots\cdots (82)$$

where $r_{\mathrm{j}\omega}(t)$ can only contains a single frequency at each frequency. The performance frequency gain of the continuous-time tracking error is shown in Figure 6. It shows that the approaches that do not compensate for oscillating poles of the feedforward controller due to discretization make large errors around Nyquist frequency. In low frequency, $|E_r|$ is smaller in order of Case 1 < Case 5 = Case 7 < Case 3 < Case 2. From these analysis, Case 2, 3, 5, and 7 are preferable approaches.

**5.3 Verification in time domain** The time domain verification is conducted in the continuous-time reference trajectory that is shown in Figure 7. The time series error $e(t)$ in simulation with sampling time $0.1\delta = 0.4$ ms is shown in Figure 8. Root Mean Square error $e_{\mathrm{RMS}} = \mathrm{RMS}(e(t))$ is shown in Table 1. The result shows that Case 2 achieves the best intersample performance because the reference signal excites up to Nyquist frequency and Case 2 has enough high sampling frequency compared to (anti) resonance frequencies.

## 6. Conclusion

In this paper, perfect tracking control approaches are described focusing on intersample performance in multi-modal motion systems. The model of the multi-modal motion system is decomposed into combinations of the states that can be selected for the perfect tracking control. The verification in a

Table 1. Root Mean Square error $e_{\mathrm{RMS}}$ in each approach. $T_r$ is the reference sampling time. $G_{c,mr}$ and $G_{c,sr}$ are the continuous-time model for the multirate and single-rate inversion.

| Case | Line | Approach | $T_r$ | $G_{c,mr}$ | $G_{c,sr}$ | $e_{\mathrm{RMS}}$ [µm] |
|---|---|---|---|---|---|---|
| 1 | | Single-rate Feedforward | $\delta$ | - | $G_c$ | 1.1454 |
| 2 | | Multirate Feedforward | $4\delta$ | $G_c$ | - | 0.3292 |
| 3 | | Additive Decomposition | $2\delta$ | $G_{c,mod,1}$ | - | 0.3868 |
| 4 | | Additive Decomposition | $2\delta$ | $G_{c,mod,2}$ | - | 13.4153 |
| 5 | | Multiplicative Decomposition | $2\delta$ | $N_1/D_1$ | $N_2/D_2$ | 0.3688 |
| 6 | | Multiplicative Decomposition | $2\delta$ | $N_2/D_1$ | $N_1/D_2$ | 1.1555 |
| 7 | | Multiplicative Decomposition | $2\delta$ | $N_1/D_2$ | $N_2/D_1$ | 0.3688 |
| 8 | | Multiplicative Decomposition | $2\delta$ | $N_2/D_2$ | $N_1/D_1$ | 1.1555 |

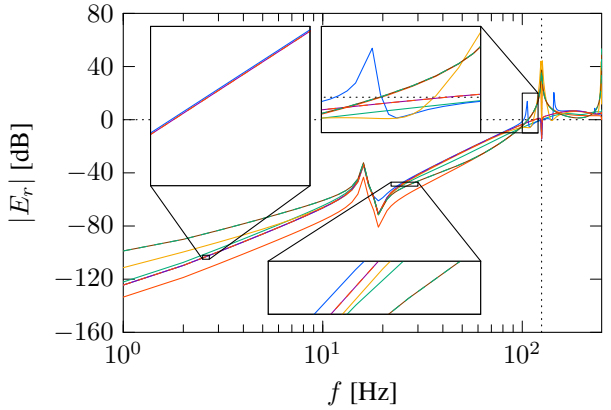


Fig. 6. Performance frequency gain of the continuous–time tracking error. Nyquist frequency is shown in a vertical black dotted line (⋯⋯).

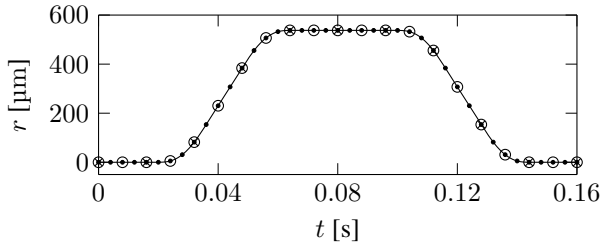


Fig. 7. Continuous-time 4th order polynomial trajectory reference $r(t)$. (•), (○), and (×) show sampling points every $\delta$, $2\delta$, and $4\delta$.

multi-modal motion system shows that state tracking should be used to compensate for the oscillating poles of the feedforward controller due to discretization. Ongoing research focuses on the optimal mode selection when the sampling frequency is not enough high for the (anti) resonance frequencies and robust performance against the modeling error.

## References


( 1 ) M. Tomizuka, "Zero Phase Error Tracking Algorithm for Digital Control," *Journal of Dynamic Systems, Measurement, and Control*, vol. 109, no. 1, p. 65, 1987.

( 2 ) M. Steinbuch, T. Oomen, and H. Vermeulen, "Motion Control, Mechatronics Design, and Moore's Law," *IEEJ Journal of Industry Applications*, vol. 2, no. 4, p. 21006010, 2021.

( 3 ) M. Poot, J. Portegies, N. Mooren, M. van Haren, M. van Meer, and T. Oomen, "Gaussian Processes for Advanced Motion Control," *IEEJ Journal of Industry Applications*, no. 41, p. 21011492, 2022.

( 4 ) T. Hayashi, H. Fujimoto, Y. Isaoka, and Y. Terada, "Projection-based Iterative Learning Control for Ball-screw-driven Stage with Consideration of Rolling Friction Compensation," *IEEJ Journal of Industry Applications*, vol. 9, no. 2, pp. 132–139, mar 2020.

( 5 ) K. Åström, P. Hagander, and J. Sternby, "Zeros of sampled systems," *Automatica*, vol. 20, no. 1, pp. 31–38, jan 1984.

( 6 ) J. van Zundert and T. Oomen, "On inversion-based approaches for feedforward and ILC," *Mechatronics*, vol. 50, no. November 2016, pp. 282–291, apr 2018.

( 7 ) H. Fujimoto, Y. Hori, and A. Kawamura, "Perfect tracking control based on multirate feedforward control with generalized sampling periods," *IEEE Transactions on Industrial Electronics*, vol. 48, no. 3, pp. 636–644, jun 2001.

( 8 ) W. Ohnishi, T. Beauduin, and H. Fujimoto, "Preactuated Multirate Feedforward Control for Independent Stable Inversion of Unstable Intrinsic and Discretization Zeros," *IEEE/ASME Transactions on Mechatronics*, vol. 24, no. 2, pp. 863–871, apr 2019.

( 9 ) W. Ohnishi and H. Fujimoto, "Multirate Feedforward Control Based on Modal Form," in *2018 IEEE Conference on Control Technology and Applications (CCTA)*, no. 2. IEEE, aug 2018, pp. 1120–1125.

(10) M. Mae, W. Ohnishi, and H. Fujimoto, "Multirate Feedforward Control based on Modal Form with Mode Selection Applied to Multi-Modal High-Precision Positioning Stage," in *2021 IEEE International Conference on Mechatronics (ICM)*. IEEE, mar 2021, pp. 1–6.

(11) J. van Zundert, W. Ohnishi, H. Fujimoto, and T. Oomen, "Improving Intersample Behavior in Discrete-Time System Inversion: With Application to LTI and LPTV Systems," *IEEE/ASME Transactions on Mechatronics*, vol. 25, no. 1, pp. 55–65, feb 2020.

(12) T. Chen and B. A. Francis, *Optimal Sampled-Data Control Systems*. London: Springer London, 1995.

(13) W. K. Gawronski, *Advanced Structural Dynamics and Active Control of Structures*. New York: Springer, 2004.


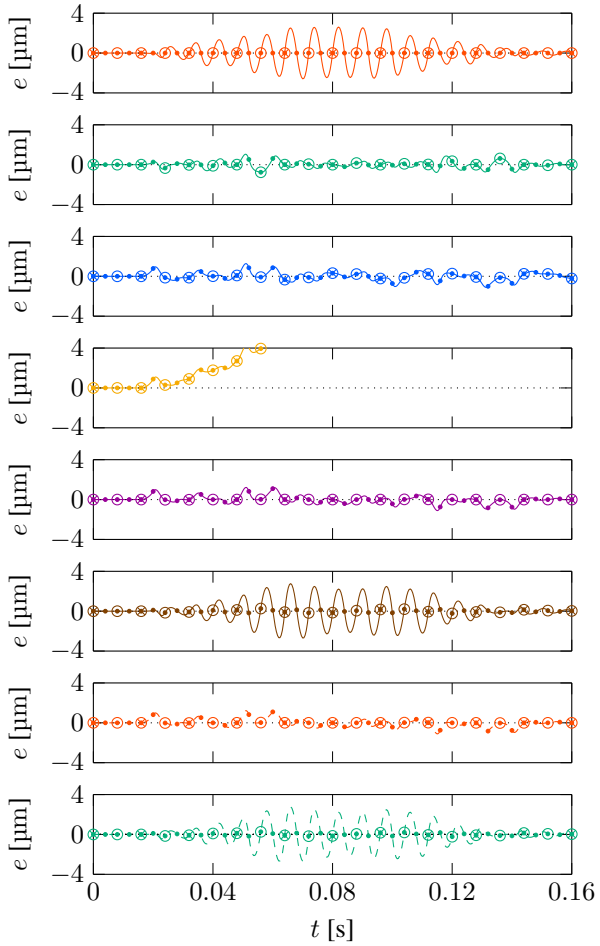


Fig. 8. Error $e(t)$ in simulation with sampling time $0.1\delta = 0.4$ ms. (•), (○), and (×) show sampling point every $\delta$, $2\delta$, and $4\delta$.